J Mater Sci (2007) 42:9083–9091
DOI 10.1007/s10853-006-0957-z

Study on the non-isothermal crystallization behaviors of PA6/silica nanocomposites prepared by the sol–gel process

Caixian Zhao · Ping Zhang · Shaorong Lu · Jiangping He · Xiayu Wang

Received: 26 May 2005 / Accepted: 8 September 2006 / Published online: 20 July 2007

Abstract A organic–inorganic PA6/partially functionalized silica hybrid nanocomposites was prepared by caprolactam polymerized and silica nanoparticles in situ gernerated through condensation of partially functionalized silicic acid, which was prepared through hydrolysis of tetraethoxysilane (TEOS) and 3-glycidoxypropyltrimethoxysilane (GPTES), in one process. The non-isothermal crystallization behaviors of pure PA6, PA6/unfunctionalized silica (PA6S) and PA6/functionalized silica (PA6FS) hybrid materials were investigated by differential scanning calorimetry (DSC). Two methods, namely, the Avrami and the Mo, were applied to describe the crystallization process of these three materials. DSC results showed that the crystallization rates of PA6FS is faster than that of pure PA6 and PA6S at the same cooling rate, the nano-silica particles functionalized by GPS in hybrid material acted as more effective nucleation agents, and the crystallization rates of all these samples increased with the cooling rate increasing. XRD results indicated that the addition of functionalized nano-silica particles favored the formation of the γ crystalline form.

C. Zhao · S. Lu · J. He · X. Wang (✉)
Institute of Polymer Science & Engineering, Xiangtan University, Xiangtan 411105 Hunan Province, P.R. China
e-mail: wxy@xtu.edu.cn

C. Zhao · P. Zhang · S. Lu · J. He · X. Wang
Key Laboratory of Advance Materials and Rheological Properties, Ministry of Education, Xiangtan 411105 Hunan Province, P.R. China

C. Zhao · P. Zhang
Insitute of Fundamental Mechanics and Material Engineering, Xiangtan University, Xiangtan 411105 Hunan Province, P.R. China

Introduction

In recent years, polymer-based organic–inorganic hybrid material, which considered as innovative advanced materials, has gained increasing attention in the field of material science [1–9]. In order to prepare hybrid materials with the size of inorganic particles in the nanoscale, one of the most promising composite systems is the hybrid based on the sol–gel process, which is a convenient method for preparation of hybrid materials from alkoxysilyl group containing materials via continuous reaction steps of hydrolysis and condensation catalyzed by acidic or basic catalysts [1, 2, 5, 9]. From our laboratory, we reported a novel method [9], which nanoparticles in situ generated though hydrolysis and condensation of inorganic acid and polymerization of caprolactam in one process, of prepared PA6/inorganic nanoparticles. In our previous work [10], we prepared PA6/functionalized silica hybrid nanocomposites (PA6SF) by caprolactam and partially functionalized silicic acid, which prepared by hydrolysis of TEOS and GPTES, in one process, which showed dramatic increases in mechanical properties and heat resistance. In this article, we would like to focus on the crystallization behaviors of PA6FS hybrid nanocomposites.

It is well known that the crystallization process of a polymer plays an important role in the production of composites, and it also influences directly the properties of the material. The quality of a crystal involves its morphology, crystalline structure and crystallization degree, which influence greatly the physical properties and chemical properties of the nanocomposites. The behavior of thermoplastic semi-crystalline polymers during non-isothermal crystallization from the melt is of increasing technological importance, because these conditions are the closest to real industrial processing conditions.

There are many of papers on studying the crystallization kinetics of PA6 nanocomposites [11–13], but no publication has been found concerning the crystallization kinetics of the PA6/silica hybrid nanocomposites made by functionalized silica nanoparticles in situ generated and caprolactam polymerized in one process. This study investigated the crystallization behavior of these PA6/functionalized silica hybrid nanocomposites under non-isothermal conditions. The Avrami method and the Mo method were used for the analysis. XRD was also used to clarify the crystalline structure of PA6FS hybrid nanocomposites obtained under different cooling conditions.

Experimental

Materials

ε-caprolactam was purchased from Yueyang Chemical Plant (China) without further purification. 3-glycidoxypropyltrimethoxysilane (GPTES) was purchased from Chemical Reagent Co. of wuhan University (China) and was purified by distillation before use. Tetraethoxysilane (TEOS) and ethanol (both chemical reagent grade), were ordered from Xilong Chemical Fractory, Guangdong (China).

Preparation of PA6FS hybrid nanocomposites

The PA6FS hybrid nanocomposites used in this study was prepared in three steps as follows: (1) Into a 500 mL three-necked round-bottomed flask, which was equipped with a N_2 inlet–outlet and a cooler, 117 mL TEOS, 190 mL ethanol and 13 g GPTES were added. After vigorous stirring with a magnetic at room temperature for 15 min, 36 mL 0.05 M hydrochloric acid was added. The stirring was carried out for about 30 min under ambient condition and a transparent solution was obtained; (2) 3,000 g ε-caprolactam, the solution obtained by step (1) and 1 g antioxidant were added into a reactor equipped with a mechanical stirrer. The mixture was heated to and held at 383 K for 12 h under vacuum; (3) 80 g distilled water as the initiator was added into the reactor, the mixture was heated to and held at 453–493 K for 1 h and then heated at 538 K for 5 h at 0.5~0.8 MPa in a N_2 atmosphere, then at 0~–0.06 MPa for about 1 h. The material was extruded to produce cylindrical extrudates by N_2, followed by immersed immediately in a cold-water (about 293 K) and pelletized with an adjustable rotating knife, located after water bath, into 5 mm length. Then these granules were washed with water at 357 K for 10 h. The chemical reactions of the synthesis of PA6FS hybrid nanocomposites are shown in Scheme 1. Pure PA6 and PA6S (prepared by reported [9]) hybrid nanocomposites were also prepared under the same condition.

Differential scanning calorimetry measurement

The non-isothermal analyses were carried out using a TA DSC-Q10 differential scanning calorimeter thermal analyzer. The samples were heated to 523 K at a rate of 20 K/min under nitrogen atmosphere, then kept for 5 min at this temperature to eliminate the heat history before cooling at a specified cooling rate. Constant cooling rate

Scheme 1

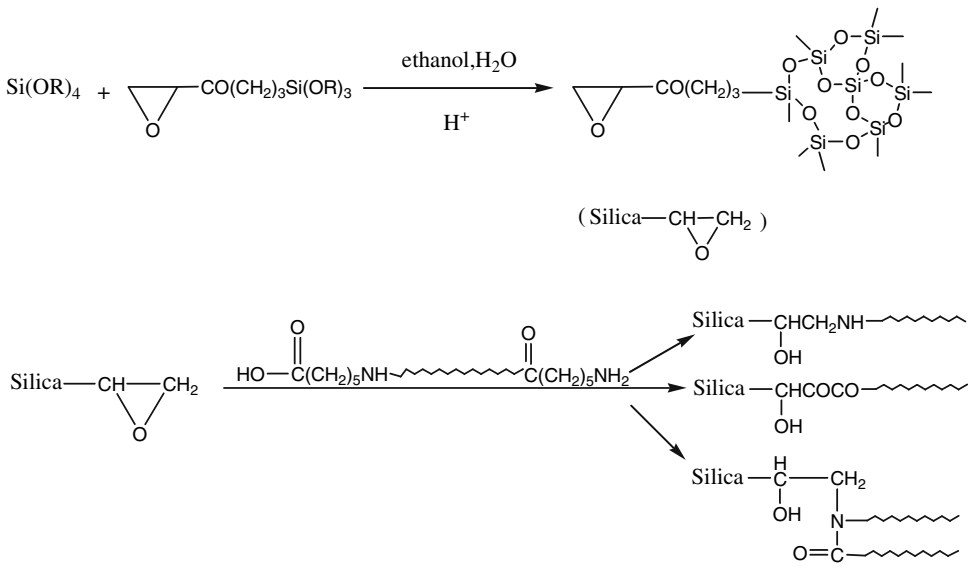

2.5, 5, 10, 15, 20 and 40 K/min were applied. The thermograms corresponding to the heating and cooling cycles were recorded and analyzed to estimate the non-isothermal crystallization kinetics and crystallinity degree.

Transmission electron microscope (TEM) observation

Thin plates were cut by ultramicrotomy from the systems and observed under a TECNAI G^2 20 Transmission Electron Microscope (TEM) at a high voltage of 120 kV.

X-ray diffraction (XRD)

To eliminate the influence of the specimen thickness, about 100 μm films of PA6 and PA6FS were prepared as reported [8]: The granules of PA6 and PA6FS were put between two glass slides, and were heated in oil-bath up to 523 K. After the granules entirely melted, a load was applied on the surfaces of the slides to press the melted materials into thin films. These films were kept on 523 K for 5 min to eliminate the heat history, then cooled under three kinds of conditions: (1) The films were cooled down in the oil-bath from 523 K to 293 K naturally; (2) The films were cooled down in the air at 293 K; (3) The films were quenched in the water at 293 K.

XRD patterns were recorded by a D/max 2550 X-ray diffractometer. The CuKα radiation source was operated at 40 kV and 300 mA. Patterns were recorded by monitoring those diffractions from 5° to 40°. The scan speed was 4°/min.

Non-isothermal crystallization kinetics model

It is well known that isothermal crystallization kinetics of polymers is commonly studied by the Avrami method [14]

$$1 - X_c(t) = \exp(-Z_t t^n) \tag{1}$$

where $X_c(t)$ is the relative crystallinity degree, n is the Avrami crystallization exponent dependent on the mechanism of nucleation, t is the time taken during the crystallization process, and Z_t is a crystallization growth rate constant. Both Z_t and n are constants which are denoted as a given crystalline morphology and type of nucleation at a particular crystallization condition. Therefore, we have

$$\log[-\ln(1 - X_c(t))] = \log Z_t + n \log t \tag{2}$$

Plotting $\log[-\ln(1 - X_c(t))]$ versus $\log t$ for a certain cooling rate, the Avrami exponent n and the crystallization rate Z_t can be calculated. Equation (1) is suitable for an isothermal crystallization system. Just like isothermal analysis, non-isothermal crystallization can also be analyzed by the Avrami equation, but, considering the non-isothermal characterization, Jeziorny [15] presented the final form of the parameter characterizing the kinetics of non-isothermal crystallization as follows:

$$\log Z_c = \log Z_t / \phi \tag{3}$$

where ϕ is the cooling rate.

The non-isothermal crystallization can also be analyzed using the Ozawa method [16]. The Ozawa equation is as follows

$$1 - X_c = \exp[-k(T)/\phi^m] \tag{4}$$

where $k(T)$ is the crystallization rate constant, X_c is the relative crystallinity, ϕ is the cooling rate, and m is the Ozawa exponent depending on the crystal growth and nucleation mechanism.

Mo and Liu [17, 18] have proposed a new kinetic equation of non-isothermal crystallization by combing the Avrami and Ozawa equations:

$$\log \phi = \log F(T) - a \log t \tag{5}$$

where a refers to the ratio of the Avrami exponent n to the Ozawa exponent $m(a = n/m)$; the parameter $F(T) = [K(T)/Z_t]^{1/m}$ represents the value of cooling rate, which has to be chosen at unit crystallization time when the measured system amounts to a certain degree of crystallinity. According to Eq. 5, the plot of $\ln\phi$ versus $\ln t$ at a given crystallinity will be a straight line. Parameters a and $F(T)$ can be obtained from the slope and the intercept of the line.

Results and discussion

Morphologies of SiO_2

TEM photographs of PA6S and PA6FS are shown in Fig. 1. Figure 1a shows that the silica nanoparticles were approximately 50~70 nm in diameter, the nanoparticles formed a slightly aggregated and became larger in size, and dispersion of the particles in PA 6 was poor. However, the size silica in the PA6FS is 30 nm, this indicates that the silica particles exhibited a homogenous matrix. The reason for this is possible that GPTES used as a coupling agent has an epoxy group and this group reacted with PA6 matrix. These results mean that the fine silica particles are composed of silica and a part of epoxy network which should form an interpenetrating network structure between the

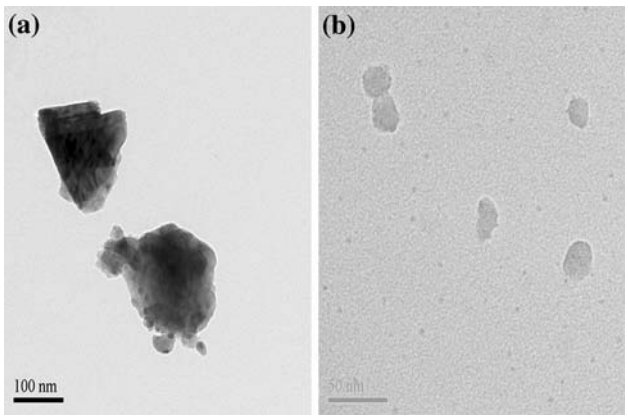

Fig. 1 TEM graphs of PA6S (**a**) and PA6FS (**b**)

organic and inorganic components with a covalent bond. It suggested that the GPTES coupling agent resulted in the morphological change of the hybrid materials.

Non-isothermal crystallization behavior

The DSC thermograms of non-isothermal crystallization for pure PA6, PA6S and PA6FS hybrid nanocomposites at different cooling rates are presented in Figs. 2–4, respectively. Figure 2 reveals a small crystallization exotherm at 455.5 K(T_p) for pure PA6 cooled at 2.5 K/min, T_p peak became more intense and shifts to lower temperature as the cooling rate increases. A similar trend was observed in PA6S (Fig. 3) and PA6FS (Fig. 4) hybrid nanocomposites. The values of T_p, T_i (initial crystallization temperature) and ΔH (the crystallization enthalpy) of non-isothermal crystallization exotherms of these three materials were listed in Table 1. It is clear that all the samples have nearly same T_i, which means the addition of silica nanoparticles has little

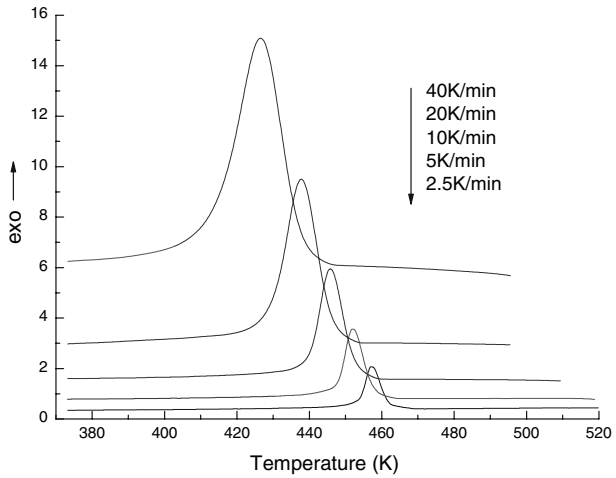

Fig. 3 DSC thermograms of non-isothermal crystallization for PA6S nanocomposites at different cooling rates

effect on the onset temperature of the crystallization. As for the ΔH, which is proportional to the degree of crystallinity X_c, it can be seen that the value change in the following order: pure PA6 > PA6S > PA6FS.

Table 1 listed the value of the crystallization peak time t_p, which is denoted as the time the sample spends during the temperature drop from T_i to T_p. The t_p decreases roughly with the increase of the cooling rate, meaning the increase in the rate of crystallization. It can also be seen that the value of t_p of PA6FS is smaller than that of pure PA6, indicating that the crystallization of pure PA6 is more difficult than that of PA6FS hybrid nanocomposites. For comparison, the reciprocal values of the time t_p versus cooling rates for all the samples were plotted in Fig. 5. It was found that for a t_p certain sample, the rate of non-isothermal crystallization increases with increasing the

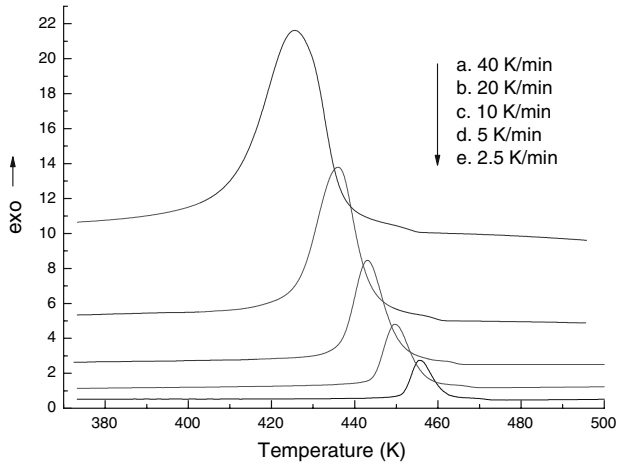

Fig. 2 DSC thermograms of non-isothermal crystallization for pure PA6 at different cooling rates

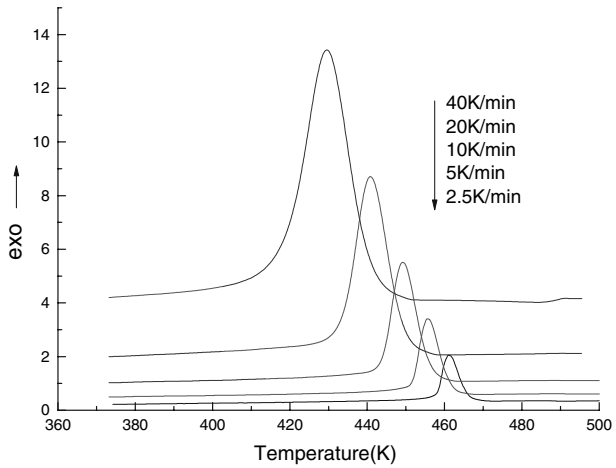

Fig. 4 DSC thermograms of non-isothermal crystallization for PA6FS nanocomposites at different cooling rates

Table 1 Values of ΔH, T_i, T_p and t_p at various cooling rates for pure PA6, PA6S and PA6FS

R (K/min)	ΔH (J/g)	T_i (K)	T_p (K)	t_p (min)
Pure PA6				
2.5	60.62	472.7	455.5	6.9
5	59.76	469.5	449.6	4.0
10	57.15	465.8	443.1	2.3
20	54.40	461.5	436.0	1.3
40	53.7	455.7	425.6	0.8
PA6S				
2.5	48.36	469.5	457.0	5
5	45.80	465.1	452.0	2.7
10	44.29	460.1	445.8	1.4
20	42.14	455.3	437.9	0.9
40	40.50	448.4	427.0	0.6
PA6FS				
2.5	50.71	473.1	467.0	2.4
5	50.85	468.9	462.2	1.3
10	51.32	465.1	456.9	0.8
20	52.10	459.7	450.4	0.5
40	53.39	454.0	442.8	0.3

cooling rate. The rate of crystallization of PA6FS is the highest one at all cooling rates, and the rate of PA6S is located between in the rates of PA6FS and pure PA6, which means the addition of silica nanoparticles in situ generated and functionalized by GPTES accelerates crystallization greatly.

Figures 6, 7 and 8 present the relative crystallinity degree as a function of temperature for these three materials crystallized at various cooling rates. The higher the cooling rate, the lower the temperature range at which the crystallization occurs, therefore, the transformation is controlled by nucleation. In addition, all curves have approximately the same shape, indicating that only the retardation effect of cooling rate on the crystallization is observed in these curves.

Non-isothermal crystallization kinetics analyses

Figures 9, 10 and 11 present plots of $\log[-\ln(1 - X_c(t))]$ as a function of $\log t$ for pure PA6, PA6S and PA6FS, respectively. The parameters n, Z_t, Z_c and $t_{1/2}$ showed in Table 2 were obtained from Figs. 9–11. n values of pure PA6 vary from 2.56 to 3.11, and those of PA6S range from 2.72 to 3.56, which means the addition of silica influences

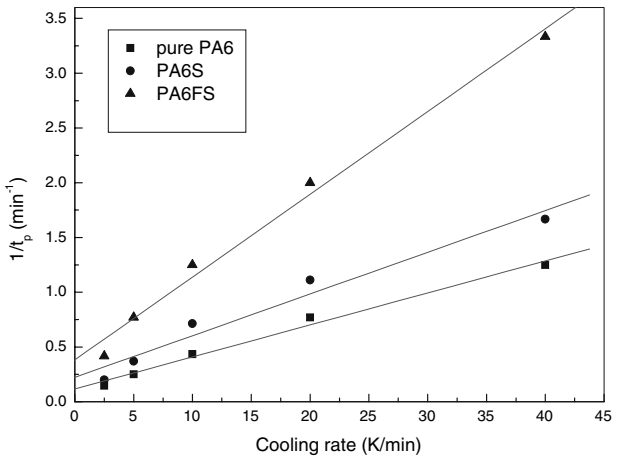

Fig. 5 Plots of $1/t_p$ as a function of cooling rate for pure PA6, PA6S and PA6FS nanocomposites

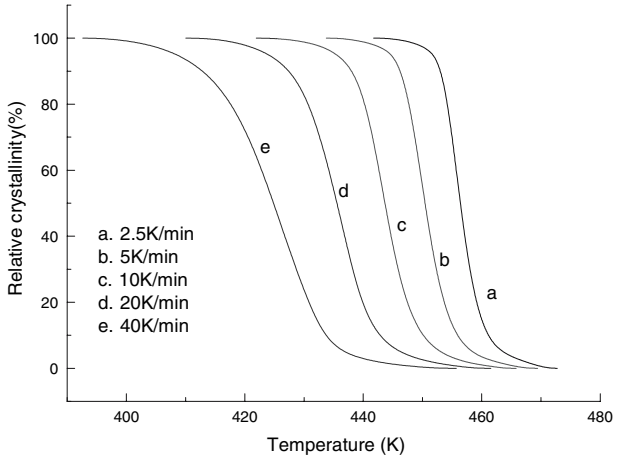

Fig. 6 Plot of relative crystallinity as a function of temperature for pure PA6 crystallized non-isothermally at various cooling rates

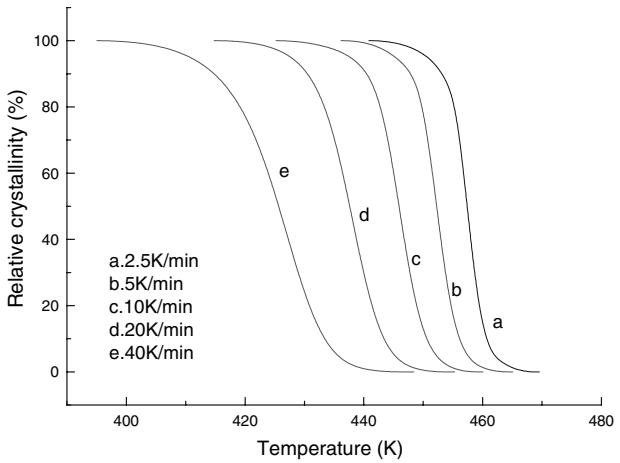

Fig. 7 Plot of relative crystallinity as a function of temperature for PA6S crystallized non-isothermally at various cooling rates

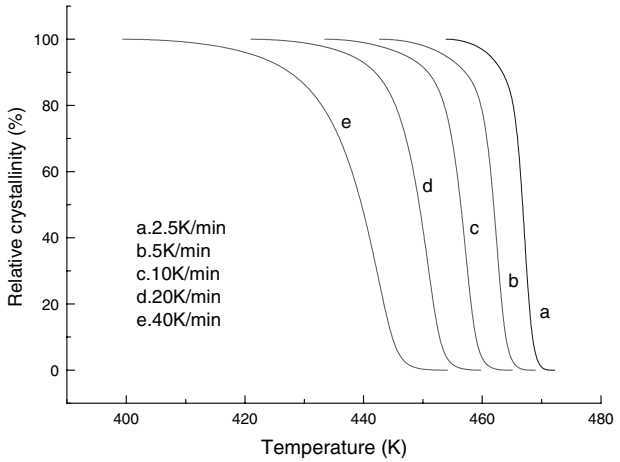

Fig. 8 Plot of relative crystallinity as a function of temperature for PA6FS crystallized non-isothermally at various cooling rates

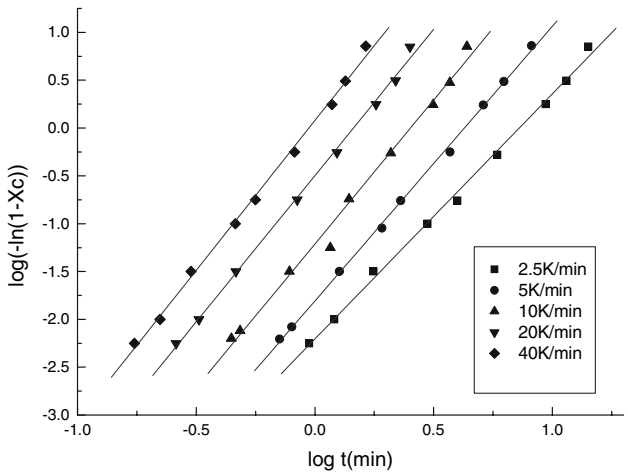

Fig. 9 Plot of log[–ln(1 – X_c)] as a function of log$t$ pure PA6

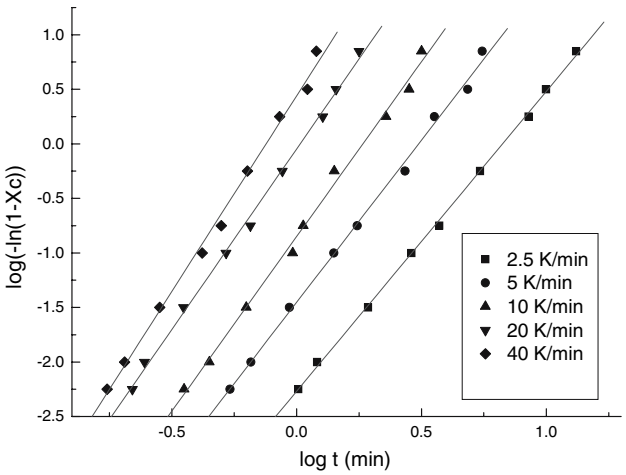

Fig. 10 Plot of log[–ln(1 – X_c)] as a function of log$t$ for PA6S

the mechanism of nucleation and the growth of PA6 crystallites. Those of PA6FS range from 2.95 to 3.91, which means the addition of silica nanoparticles in situ functionalized is more effective than that of unfunctionalized silica. The data listed in Table 2 also show that for all samples Z_c increases and $t_{1/2}$ decreases as the cooling rate increases, which means an increase of the rate of crystallization. At the same cooling rate, the higher Z_c of PA6FS than that of pure PA6 and PA6S indicates that the silica modified by GPTES prompted crystallization effectively.

Figures 12, 13 and 14 present plots of logϕ as a function of log$t$ for pure PA6, PA6S and PA6FS, respectively. The slope a and intercept log $F(T)$ showed in Table 3 were obtained from the fitted straight line. It can be seen from Table 3 that the values of $F(T)$ systematically increase with an increase in the relative degree of crystallinity. At a given degree of crystallinity, the higher the $F(T)$ value, the higher cooling rate is needed within unit crystallization time, indicating the difficulty of polymer crystallization. By comparing the values of $F(T)$ of different samples, we have

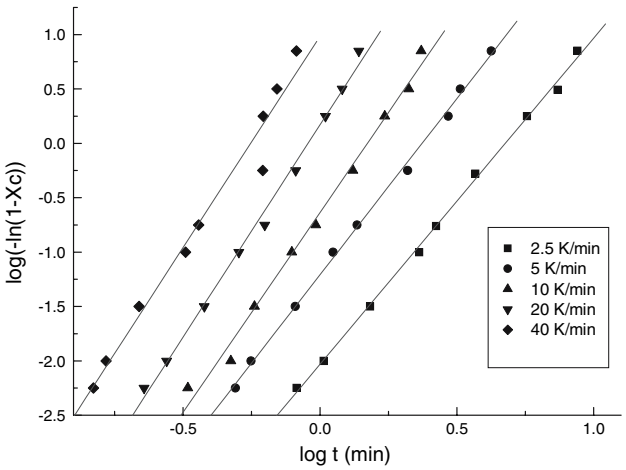

Fig. 11 Plot of log[–ln(1 – X_c)] as a function of log$t$ for PA6FS

Table 2 Values of n, Z_t, Z_c and $t_{1/2}$ at various cooling rates for pure PA6, PA6S and PA6FS nanocomposites

ϕ (K/min)	n	Z_t	Z_c (min^{-n})[a]	$t_{1/2}$ (s)
Pure PA6				
2.5	2.56	0.01	0.13	392
5	2.87	0.02	0.44	230
10	2.99	0.07	0.76	134
20	3.02	0.30	0.94	79
40	3.11	1.33	1.01	47
PA6S				
2.5	2.72	0.01	0.13	291
5	2.98	0.04	0.51	154
10	3.21	0.14	0.82	85
20	3.33	1.41	1.02	53
40	3.56	6.83	1.05	31
PA6FS				
2.5	2.95	0.07	0.35	129
5	3.23	0.17	0.70	84
10	3.68	1.54	1.04	52
20	3.91	7.52	1.11	31
40	3.86	85.22	1.12	21

[a] Is calculated from Eq. 3

found that the value of PA6FS is lower than those of pure PA6 and PA6S, meaning that the crystallization rate of PA6FS is faster than those of pure PA6 and PA6S. This is in accordance with the result obtained from the Avrami approach.

Crystalline form

PA6 is known to crystallize into various phases: the α stable crystal and among others the γ-phase [8, 19]. In the α-phase the hydrogen bonds are formed between antiparallel chains whereas in the γ-phase they are formed between parallel chains. XRD was used to gain insight into the influence of silica on the crystalline fraction. It was previously reported [20] that the α form exhibited two reflection peaks at $2\theta \approx 20°$ [α1 (200), d = 0.44 nm] and 24° [α2 (002), d = 0.37 nm], where only one reflection peak at $2\theta \approx 21°$ [γ (200), d = 0.42 nm] was observed for the γ form. The α1 peak is sensitive to the distance between hydrogen-bonded chains inside the sheet-like structures whereas the α2 peak is sensitive to the separation distance between the sheets [21].

Figures 15 and 16 show the XRD patterns of pure PA6 and PA6FS hybrid nanocomposites under different cooling conditions, respectively. The results indicate that in the

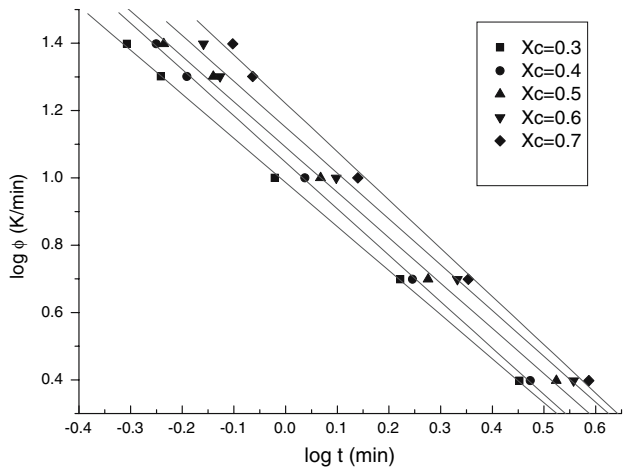

Fig. 12 Plot of logϕ as a function of log$t$ for pure PA6

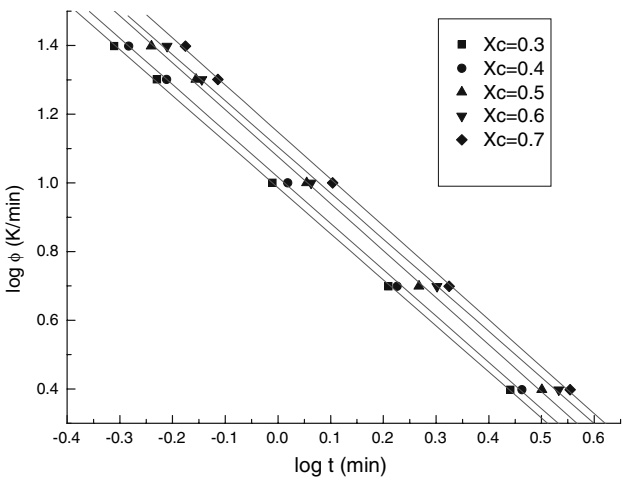

Fig. 13 Plot of logϕ as a function of log$t$ for PA6S nanocomposites

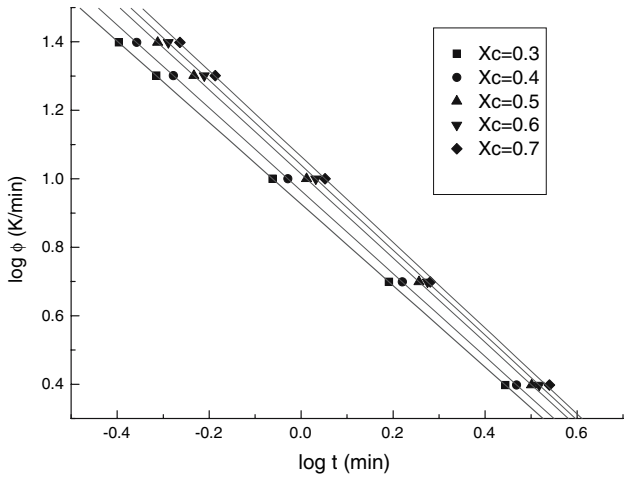

Fig. 14 Plot of logϕ as a function of log$t$ for PA6FS nanocomposites

Table 3 Values of $F(T)$ and a at various relative crystallinity for pure PA6, PA6S and PA6FS

Xc	$F(T)$	a
Pure PA6		
0.3	9.68	1.30
0.4	11.21	1.32
0.5	12.29	1.32
0.6	13.53	1.34
0.7	15.75	1.36
PA6S		
0.3	9.75	1.32
0.4	10.43	1.34
0.5	11.85	1.35
0.6	12.77	1.35
0.7	14.36	1.37
PA6FS		
0.3	8.44	1.19
0.4	9.23	1.21
0.5	10.34	1.23
0.6	10.96	1.24
0.7	11.01	1.26

slow and the medium cooling rates (cooling in oil-bath and in air), there exists only the α form, while cooled rapidly (quenched in water), the α and γ form co-existed in pure PA6 (Fig. 15). The α and γ form coexist in PA6/modified silica hybrid nanocomposites films under air cooling rate. But the γ form becomes dominant in higher cooling rate (Fig. 16). Under cooling in oil-bath, in pure PA6, the α1 peak is higher than the α2 peak (Fig. 15, curve 1). However, in PA6/modified silica hybrid nanocomposites film, the α1 peak is lower than the α2 peak (Fig. 16, curve 1). This means that the extent of hydrogen-bonded NH associated with the α-phase in PA6FS hybrid nanocomposites is

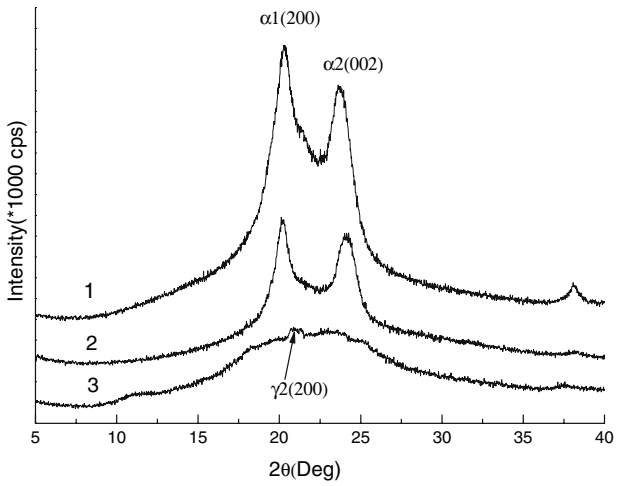

Fig. 15 XRD patterns of pure PA6 under various cooling conditions: (1) oil-bath cooling, (2) air cooling and (3) water cooling; the curves were vertically offset for clarity

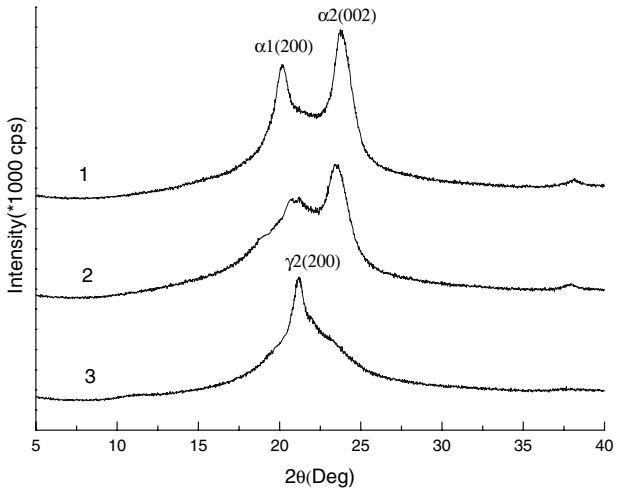

Fig. 16 XRD patterns of PA6FS nanocomposites under various cooling conditions: (1) oil-bath cooling, (2) air cooling and (3) water cooling; the curves were vertically offset for clarity

reduced [8]. Vaia et al. [22] suggested that the addition of silicate clay layers forces the amide groups of PA6 out of the plane formed by the chains. This results in conformational changes of the chains, which limits the formation of H-bonded sheets and the γ-phase is favored. We think that the same reason result in the γ-phase is favored in PA6FS hybrid nanocomposites.

Conclusion

A systematic study of the non-isothermal crystallization kinetics of pure PA6, PA6S and PA6FS has been performed by the DSC technique. The crystallization kinetics of each sample was investigate according to two different

kinetic models, namely, the Avrami and the Mo. Both models can describe the experimental data very well.

The DSC results imply that the nano-sized SiO_2 in situ generated and functionlized by GPTES in PA6FS hybrid nanocomposites act as nucleation agents and accelerates the crystallization during the cooling process from the melt. But the introduction of silica nanoparticles does not have great effect on the onset temperature of crystallization. The addition of silica influences the mechanism of nucleation and the growth of polyamide crystallites.

XRD results indicated that the addition of functionalized nano-silica particles favored the formation of the γ crystalline form.

Acknowledgements The financial support from the National Natural Science Foundation of China (No. 10372087), Scientific Research Fund of Hunan Provincial Education Department (No. 05B004) and the College Student's Innovation Foundation of Xiangtan University is greatly acknowledged.

References

1. Schmidt H (1985) Non-cryst Solids 73:681
2. Wen JY, Wilkes GL (1996) Chem Mater 8:1667
3. Yang F, Ou YC, Yu ZZ (1998) J Appl Polym Sci 69:355
4. Balazs AC, Singh C, Zhulina E (1998) Macromolecules 31:8370
5. Hajji P, David L, Gerard JF, Paul C (1999) J Polym Sci B37:3172
6. Reynaud E, Jouen T, Gauthier C, Vigier G, Varlet J (2001) Polymer 42:8759
7. Li Y, Yu J, Guo ZX (2002) J Appl Polym Sci 84:827
8. Wu QJ, Liu XH, Lars AB (2002) Polymer 43:2445
9. Zhang P, Wang XY, Wei SS (2004) A direct method for synthesize PA6/inorganic nanocomposites. China Patent: ZL021398369.4
10. Zhao CX, Zhang P, He JP, Lu SR, Wang XY (2007) Poly Mater Sci Eng (Chinese) 23(1):218
11. Liu XH, Wu QJ (2002) Eur Poly J 38:1383
12. Fornes TD, Paul DR (2003) Polymer 44:3945
13. Tol RT, Mathot VBF, Groeninckx G (2005) Ploymer 46:2955
14. Avrami M (1940) J Chem Phys 8:212
15. Celina M, George GA (1995) Degrad Stab 48:297
16. Ozawa T (1971) Polymer 12:150
17. Liu JP, Mo ZS (1991) China Polym Bull (in Chinese) 4:199
18. Liu TX, Mo ZS, Wang SG et al (1997) Polym Eng Sci 37:568
19. Men YF, Rieger J (2004) Euro Poly J 40:2629
20. Campoy I, Gómez MA, Marco C (1998) Polymer 39:6279
21. Murthy NS, Curran SA, Aharoni SM, Minor H (1991) Macromolecules 24:3215
22. Lincoln DM, Vaia RA, Wang ZG, Hsiao BS (2001) Polymer 42:1621